LHCb-PUB-2018-006
May 11, 2018

Triggering $B_s^0 \to \gamma\gamma$ at LHCb

Sean Benson[1], Albert Puig[2].

[1] *Nikhef National Institute for Subatomic Physics, Amsterdam, The Netherlands*
[2] *Universität Zürich, Zürich, Switzerland*

Abstract

The trigger strategy used in the search for the $B_s^0 \to \gamma\gamma$ decay in Run 2 is described. A sample of data is also provided, corresponding to $80\,\text{pb}^{-1}$ of diphoton candidates collected in 2015.

1 Introduction

The $B^0_{(s)} \to \gamma\gamma$ decay is a $b \to d(s)\gamma\gamma$ transition described by an annihilation topology. It is sensitive to contributions from physics beyond the Standard Model (SM) including a fourth generation [1], an extended Higgs sector [2] and SUSY [3]. Previous measurements by the Belle and BaBar collaborations have set limits of $\mathcal{B}(B^0_s \to \gamma\gamma) < 8.7 \times 10^{-6}$ at 90 % confidence level (CL) [4] and $\mathcal{B}(B^0 \to \gamma\gamma) < 3.3 \times 10^{-7}$ at 90 % CL [5], which are significantly above the SM predictions of $\mathcal{B}(B^0_s \to \gamma\gamma) \sim (2 - 37) \times 10^{-7}$ and $\mathcal{B}(B^0 \to \gamma\gamma) \sim (1 - 10) \times 10^{-8}$ [6].

The study of these purely neutral modes at LHCb is challenging, but the use of photon conversions, which happen for around 25 % of photons, provides handles to reduce the background levels. With offline selections already in place since Run 1, this note describes the trigger strategy adopted in Run 2, where a set of trigger lines were introduced to select the $\gamma\gamma$ signature for the case of zero, one, and two photon conversions.[1]

The maximum rate at which events can be read out of the detector is imposed by the front-end electronics and corresponds to a rate of 1.1 MHz. In order to determine which events are kept, hardware triggers based on field-programmable gate arrays are used with a fixed latency of 4 μs. Information from the ECAL, HCAL, and muon stations is used in separate L0 triggers. All events selected by L0 are transferred to the High Level Trigger (HLT). The HLT is a software application, executed on an event filter farm, that is implemented in the same Gaudi framework [7] as the software used for the offline reconstruction. Sections 2, 3 and 4 describe the strategy in L0, HLT1 and HLT2, respectively, where HLT1 & HLT2 are the first and second software trigger levels. A small fraction of data collected in Run 2 to illustrate the background levels faced by this search is given in Sec. 5.

Throughout the note, efficiencies are evaluated with respect to a loose offline selection, detailed in Table 1, inspired by those applied in the analysis of other radiative decays as well as the $B^0_s \to \gamma\gamma$ Stripping; even though the special topology of our signal decay makes this selection unrealistically soft, it gives a good starting point to understand the difficulties of triggering $B^0_s \to \gamma\gamma$ signatures.

2 L0

The strategy at L0 is similar to that of other radiative decays and relies on the `L0Photon` or `L0Electron` channels.[2] As shown in Table 2, the L0 efficiencies with respect to the offline selection requirements are large, even in the case of two conversions, which are picked up by the `L0Electron` line.

3 HLT1

At HLT1 level, $B^0_s \to \gamma\gamma$ decays with at least one long conversion rely on an electron candidate detected inside the VELO to pass the `Hlt1TrackMVA` HLT1 trigger line as TOS.

[1] In this note, these will be labelled as *0CV*, *1CV* (both *LL* and *DD*, corresponding to *long* and *downstream* conversions) and *2CV*, respectively.

[2] Signal events throughout this note are required to be *Trigger on Signal* (TOS) [8], *i.e.*, the signal candidate is responsible for firing the given trigger line.

Prior to 2015 data taking, calorimeter photons were not used in the first level of the software trigger [9], making it impossible to have a TOS trigger for the no-conversion case, thus decreasing its trigger efficiency. A special reconstruction algorithm designed for triggering calorimeter di-photon clusters has been included in Run 2 as part of the `Hlt1B2GammaGamma` line, and is detailed in Section 3.1. This algorithm is also capable of recovering some TOS efficiency in the *1CV DD* category, which is not triggered by `Hlt1TrackMVA` due to the lack of downstream tracking in HLT1, by triggering on one of the electrons from the conversion. The HLT1 performance for each topology is given in Table 3.

3.1 Custom di-calorimeter photon HLT1 reconstruction

Due to the limited time available for reconstruction in HLT1 it is impossible to perform full—or even partial—calorimeter reconstruction at this stage. For this reason, a dedicated algorithm has been implemented to build particles by combining the energy of two calorimeter L0 candidates and applying some basic selection requirements. Since the HLT1 line needs to execute fast, only quantities readily available from the `L0CaloCandidate`, *i.e.*, E_{T} and position are used. To save calculations, the di-photon invariant mass is approximated assuming that the distance between the two clusters is small with respect to the distance to the B vertex:

$$\begin{aligned} M^2(\gamma_1\gamma_2) &= 2E(\gamma_1)E(\gamma_2)(1-\cos\theta) \approx E(\gamma_1)E(\gamma_2)\theta^2 \\ &= \frac{E_{\mathrm{T}}(\gamma_1)D_1}{\sqrt{(x_1^2+y_1^2)}}\frac{E_{\mathrm{T}}(\gamma_2)D_2}{\sqrt{(x_2^2+y_2^2)}}\theta^2 \\ &\approx E_{\mathrm{T}}(\gamma_1)E_{\mathrm{T}}(\gamma_2)\frac{(x_1-x_2)^2+(y_1-y_2)^2}{\sqrt{(x_1^2+y_1^2)(x_2^2+y_2^2)}}, \end{aligned} \tag{1}$$

Table 1: Loose offline selection for $B_s^0 \to \gamma\gamma$ used as a baseline for the efficiency determination. The fraction of events in each category after this loose selection with respect to the total events that pass it is shown in the last row.

Variable	*0CV*	*1CV LL*	*1CV DD*	*2CV*
Calo γ CL	> 0.3	> 0.3	> 0.3	–
Calo γ p [GeV/c]	> 6	> 6	> 6	–
Calo γ E_{T} [GeV]	> 3	> 3	> 3	–
Converted γ p_{T} [GeV/c]	–	> 2.0	> 2.0	> 2.0
Converted γ M [MeV/c^2]	–	< 60	< 60	< 60
Converted γ χ^2_{IP}	–	> 4	> 0	> 1
$\sum p_{\mathrm{T},\gamma}$ [GeV]	> 6.5	> 5.5	> 5.5	> 5
B_s^0 p_{T} [GeV/c]	> 3.0	> 3.0	> 3.0	> 3.0
B_s^0 χ^2_{vtx}	–	–	–	< 20
$M_{B_s^0}$ [GeV/c^2]	$[4.3, 6.3]$	$[4.3, 6.3]$	$[4.3, 6.3]$	$[4.5, 6.1]$
Fraction of signal	83.4%	4.3%	11.7%	0.6%

Table 2: L0 efficiencies for each topology with respect to the offline selection.

Trigger requirement	$\epsilon_{0\text{CV}}$ (%)	$\epsilon_{1\text{CV LL}}$ (%)	$\epsilon_{1\text{CV DD}}$ (%)	$\epsilon_{2\text{CV}}$ (%)
`L0Electron` TOS	57.61 ± 0.30	66.9 ± 1.3	69.3 ± 0.8	79.0 ± 2.8
`L0Photon` TOS	71.68 ± 0.28	47.7 ± 1.3	49.9 ± 0.8	7.8 ± 1.9
Total L0 TOS	93.20 ± 0.15	89.7 ± 0.8	91.2 ± 0.5	80.0 ± 2.8

Table 3: HLT1 trigger efficiencies with respect to the offline selection and the L0 requirements for each topology.

Trigger requirement	$\epsilon_{0\text{CV}}$ (%)	$\epsilon_{1\text{CV LL}}$ (%)	$\epsilon_{1\text{CV DD}}$ (%)	$\epsilon_{2\text{CV}}$ (%)
`Hlt1B2GammaGamma` TOS	45.80 ± 0.32	17.1 ± 1.1	17.2 ± 0.6	9.8 ± 2.3
`Hlt1TrackMVA` TOS	–	34.2 ± 1.4	–	30 ± 4
HLT1 total	45.80 ± 0.32	43.0 ± 1.4	17.2 ± 0.6	37 ± 4

where (x_i, y_i) is the position of the cluster in the calorimeter plane and D_i its distance from the di-photon vertex, and where we have used that $D_1 \sim D_2 \sim D$ so

$$\theta^2 \approx \frac{(x_1 - x_2)^2 + (y_1 - y_2)^2}{D^2}. \tag{2}$$

With this simplification in mind, the algorithm:

1. loops over the `L0Electron` and `L0Photon` candidates;
2. filters them by their E_{T};
3. combines the remaining candidates in pairs, filters the sum of their E_{T} and performs a final filtering according to the approximate $M^2(\gamma_1\gamma_2)$ and the p_{T} of the resulting combination.

Therefore, the algorithm provides few handles for event selection, and, as a consequence, requirements need to be hard in order to keep the rate under control, as shown in Table 4. The main caveat when interpreting these selection criteria is that the energies measured at L0 (and thus in these special HLT1 candidates) correspond to a cluster of 2×2 cells, while in HLT2 and offline reconstruction at least 3×3 cells are used. Figure 1 shows a comparison between the quantities obtained using 2×2 cell clusters and their offline counterparts, without taking into account saturation effects coming from the limited dynamic range of the ECAL.[3]

4 HLT2

Multi-variate classifiers are common when implementing final selections due to the performance increase and ease of use. The application of such techniques to low-latency

[3]The L0 calorimeter E_{T} is on 8 bits and saturates at 255 ADC counts. This ADC to E_{T} conversion was set in June 2015 to be 24 MeV/ADC, so the saturation threshold is 6120 MeV. For Run 1 data, the conversion was 20 MeV/ADC, so the saturation occurred at 5100 MeV.

Table 4: Selection applied in the `Hlt1B2GammaGamma` HLT1 trigger line. Energies given here are computed with 2×2 cell clusters.

Requirement	Value
$E_{\mathrm{T}}(\gamma)$ [GeV]	> 3.5
$E_{\mathrm{T}}(\gamma_1) + E_{\mathrm{T}}(\gamma_2)$ [GeV]	> 8
$M(\gamma_1\gamma_2)$ [GeV/c^2]	$[3.5, 6.0]$
$p_{\mathrm{T}}(\gamma_1\gamma_2)$ [GeV/c]	> 2

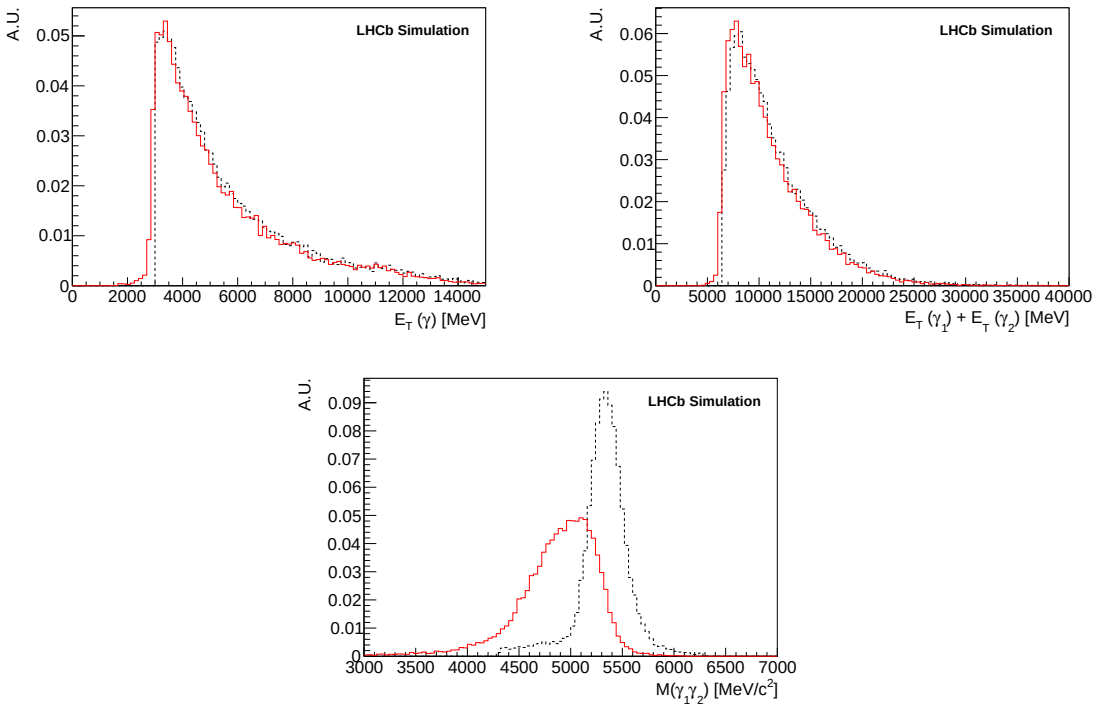

Figure 1: Comparison between 2×2 cell clusters (red solid line) and their offline counterparts (black dashed line) for variables used in the `Hlt1B2GammaGamma` HLT1 trigger line.

environments is challenging due to the time taken to evaluate the associated models. In order to use a multi-variate strategy in the LHCb online environment, a discrete BDT is implemented. This is a popular method, that is used to make multi-variate classifiers fast enough for use in real-time-analysis environments [10].

4.1 Training samples

In order to design trigger selections, simulated candidates have been used to describe the $B_s^0 \to \gamma\gamma$ distributions, while backgrounds are described using minimum bias 2015 data events.

For the case of both the signal and background training samples, the L0 hardware trigger configuration is applied and the HLT1 output is used directly as training data. Additionally, simulated signal candidates are matched to true generator level candidates. This is accomplished for the case of electrons by generating the reconstructed-generated

Table 5: Requirements on simulated candidates prior to the determination of HLT2 selections, where CL is a probability calculated from calorimeter information.

Variable	*0CV*	*1CV LL*	*1CV DD*	*2CV*
Calo γ CL	> 0.42	–	–	–
Calo γ p [GeV/c]	> 16	> 11	> 11	–
Calo γ $E_{\rm T}$ [GeV]	> 1.70	> 1.25	> 1.25	> 1.25
Converted γ $p_{\rm T}$ [GeV/c]	–	> 1.4	> 1.4	> 1.4
Converted γ $\chi^2_{\rm IP}$	–	> 1.5	–	–
B^0_s $p_{\rm T}$ [GeV/c]	> 2.0	> 1.0	> 1.0	> 1.0
B^0_s $\chi^2_{\rm vtx}$	–	–	–	< 20
$M_{B^0_s}$ [GeV/c^2]	$[4.9, 6.0]$	$[4.6, 5.8]$	$[4.6, 5.8]$	$[4.3, 5.8]$

particle relations tables from the tracks created in the trigger and the links between the detector hits and the generated particles. The generator level particle with the highest common detector hits to the reconstructed particle is used as the associated generator level candidate. For the case of neutral particles, a reconstructed photon candidate is considered as matched to a generator level candidate if the reconstructed photon shares ECAL hits with the generator level photon and the generator level photon truly originates from the decay of a B^0_s meson. The generator level information is associated to offline selected candidates, which therefore requires the offline requirements are met. These requirements are provided in Table 5. Note that these are different from the loose selection of Table 1, which is possible after a dedicated trigger selection has been introduced.

4.2 HLT2 strategy and performance

Separate classifiers are trained for each final-state topology. The topologies consist of:

- $B^0_s \to \gamma\gamma$ unconverted,
- $B^0_s \to \gamma(\to e^-e^+)\gamma$ with long conversions,
- $B^0_s \to \gamma(\to e^-e^+)\gamma$ with downstream conversions,
- $B^0_s \to \gamma(\to e^-e^+)\gamma(\to e^-e^+)$ with both long and downstream conversions.

The technique to use such multi-variate strategies in the trigger environment is to discretise the input features. In this way, output responses may be cached and quick evaluation of the model can be ensured. The discretised variables are given in Appendix A.

The following three classifiers are compared:

- *BDT*: The standard BDT using the AdaBoost algorithm.
- *BDTD*: As above, with an extra decorrelation transformation on the input variables.
- *BDTB*: A standard BDT that uses bagging rather than AdaBoost [4] .

[4]Note that bagging denotes a resampling technique where a classifier is repeatedly trained using resampled training events such that the combined classifier represents an average of the individual classifiers.

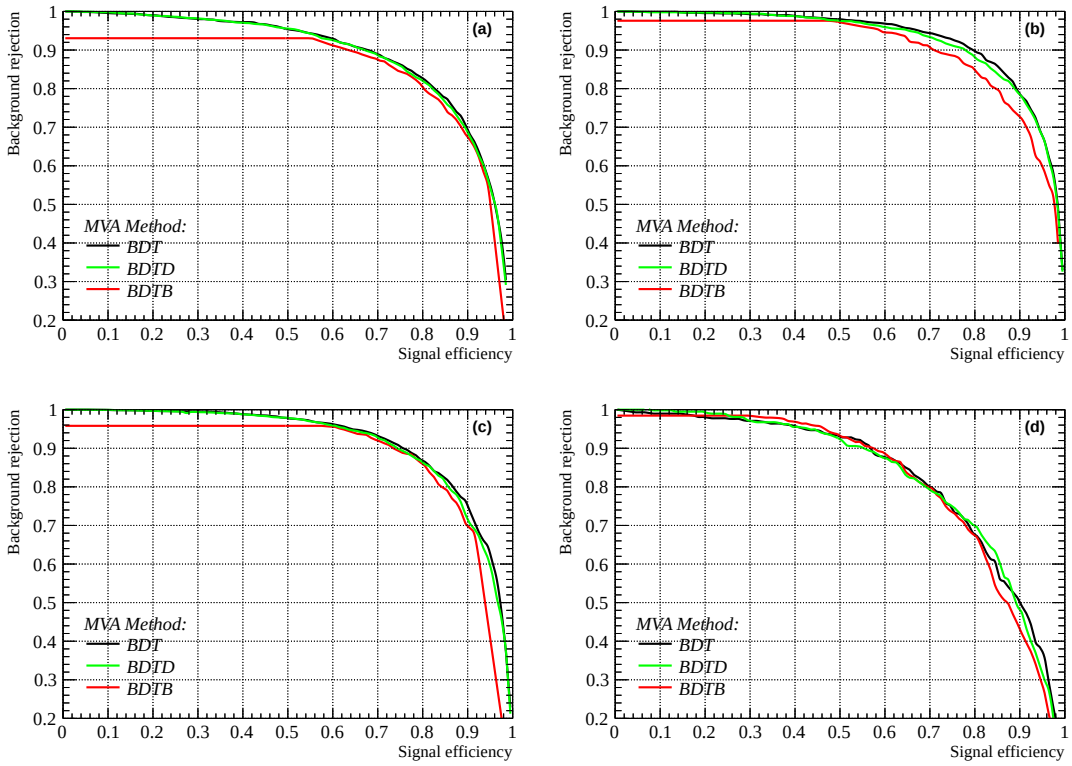

Figure 2: Efficiency versus background rejection curves for the classifiers corresponding to the di-calorimeter photon topology (a), single long conversion (b), single downstream conversion (c), and double conversion (d).

Table 6: Efficiency ϵ of the BDT classifiers with respect to L0 and HLT1 at the cut values applied in the trigger.

	0CV	*1CV LL*	*1CV DD*	*2CV*
BDT output	> 0.15	> 0.2	> 0.26	> 0.18
Signal ϵ (%)	39.8 ± 0.5	79.6 ± 1.8	73.4 ± 1.8	80.0 ± 5.0

The signal efficiency versus background rejection fraction for the three classifiers are given in Figure 2, while the BDT response distributions for the signal and background samples is given in Figure 3.

4.3 Performance

The requirements on the boosted decision trees are determined by the available rate budget. The signal efficiency performance that is most relevant is against the "Ideal" selection in Tab. 1, and it is reported, with the corresponding requirement on the BDT, in Tab. 6.

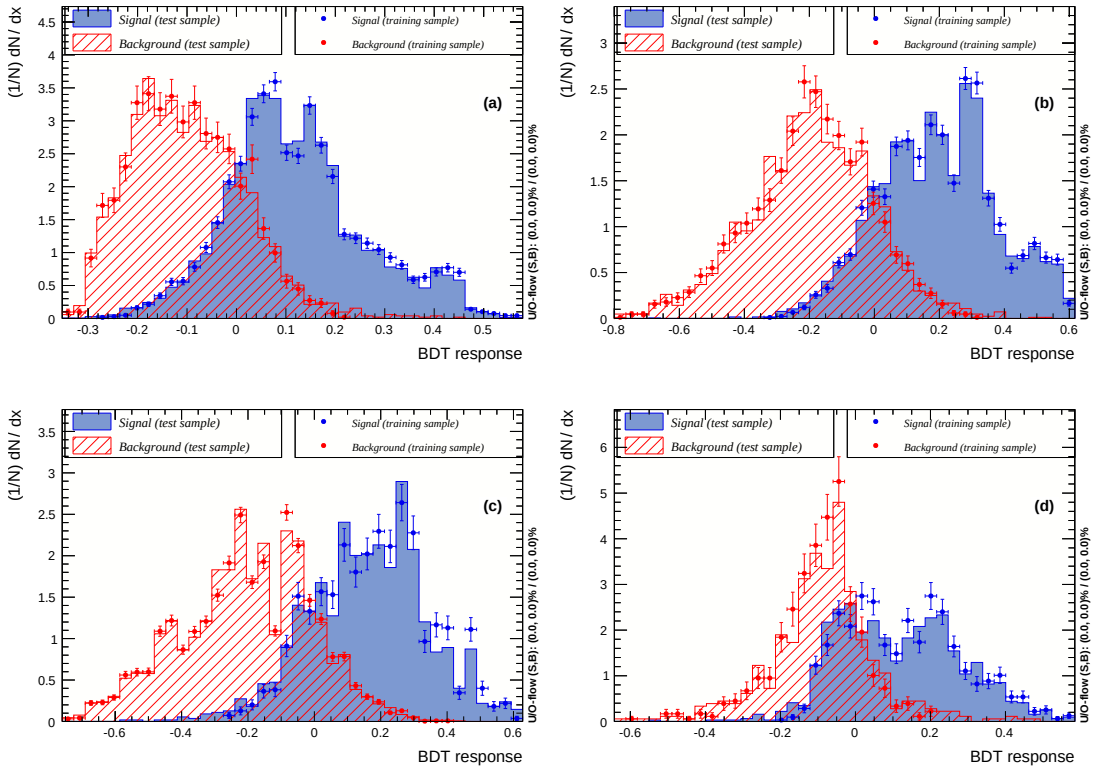

Figure 3: Signal and background BDT response distributions for the classifier corresponding to (a) the di-calorimeter photon topology, (b) single long conversion, (c) single downstream conversion, and (d) double conversion.

5 Diphoton data

Example data is provided showing real data candidates after trigger requirements. This corresponds to approximately $80\,\text{pb}^{-1}$ of data collected in 2016. The diphoton invariant mass distributions are shown in Fig. 4. The dielectron invariant mass distributions are shown in Fig. 5. For the case of the double conversion topology, the minimum value of the dielectron invariant mass is shown. In addition to showing the challenging levels of background present, Fig. 5 also serves to show that many real photons are present in the background due to the large mass peak close to zero.

Acknowledgements

We would like to thank Olivier Deschamps for his help in setting up the HLT1 di-photon line, as well as for the discussions on how to deal with the di-calorimeter photon mode. This public note is part of a project that has received funding from the European Union's Horizon 2020 research and innovation programme under the grant agreement No 747822. We acknowledge support from CERN and from the national agencies: NWO (The Netherlands), SNSF and SER (Switzerland), as well as the Swiss National Science National Science Foundation under the Ambizione project number 168169.

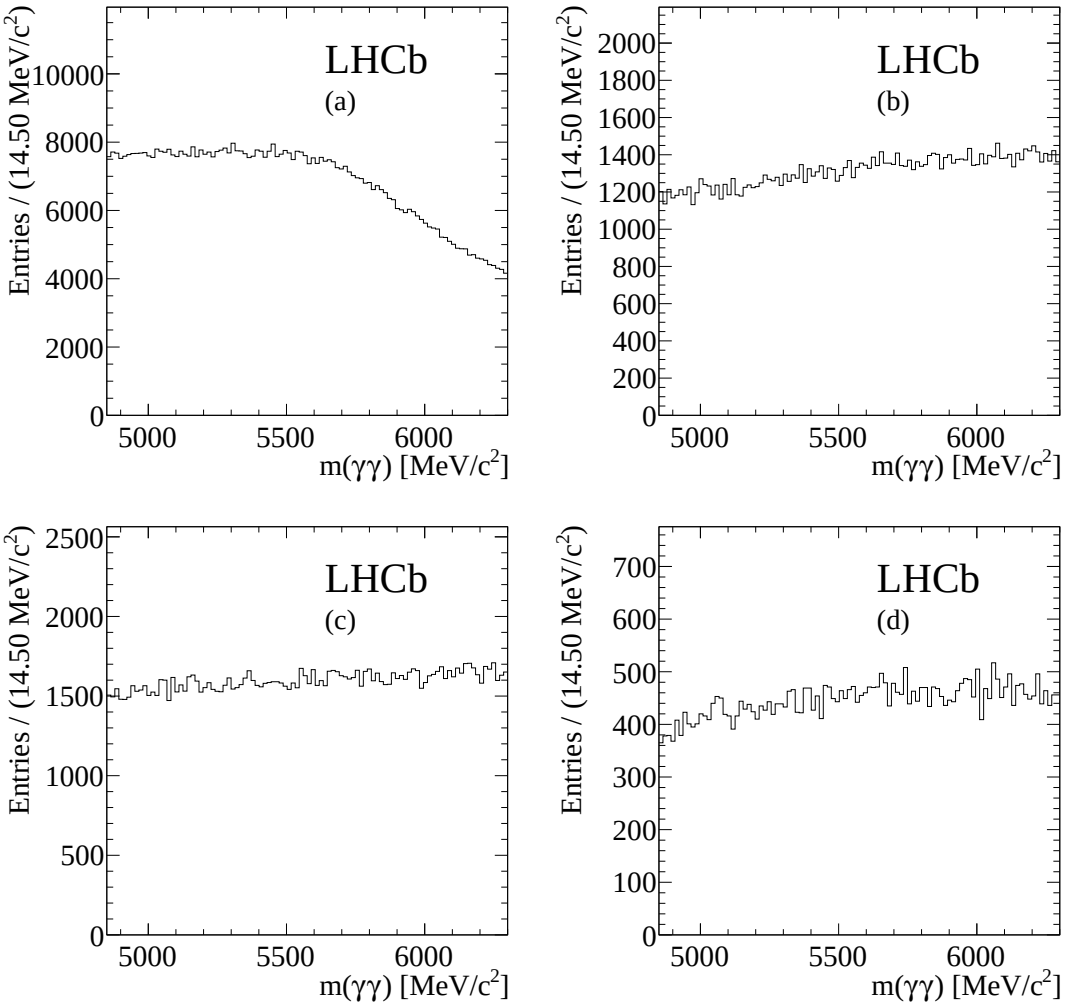

Figure 4: Diphoton invariant mass for background data events for the di-calorimeter photon (a), single long conversion (b), single downstream conversion (c), and double conversion (d) topologies.

References

[1] W.-j. Huo, C.-D. Lu, and Z.-j. Xiao, $B_{(s,d)} \to \gamma\gamma$ *decay with the fourth generation*, arXiv:hep-ph/0302177.

[2] T. M. Aliev and E. O. Iltan, $B_{(s)} \to \gamma\gamma$ *decay in the two Higgs doublet model with flavor changing neutral currents*, Phys. Rev. **D58** (1998) 095014, arXiv:hep-ph/9803459.

[3] A. Gemintern, S. Bar-Shalom, and G. Eilam, $B \to X_{(s)}\gamma\gamma$ *and* $B_{(s)} \to \gamma\gamma$ *in supersymmetry with broken R-parity*, Phys. Rev. **D70** (2004) 035008, arXiv:hep-ph/0404152.

[4] Belle, D. Dutta *et al.*, *Search for* $B_s^0 \to \gamma\gamma$ *and a measurement of the branching fraction for* $B_s^0 \to \phi\gamma$, Phys. Rev. **D91** (2015), no. 1 011101, arXiv:1411.7771.

[5] BaBar, P. del Amo Sanchez *et al.*, *Search for the Decay* $B^0 \to \gamma\gamma$, Phys. Rev. **D83** (2011) 032006, arXiv:1010.2229.

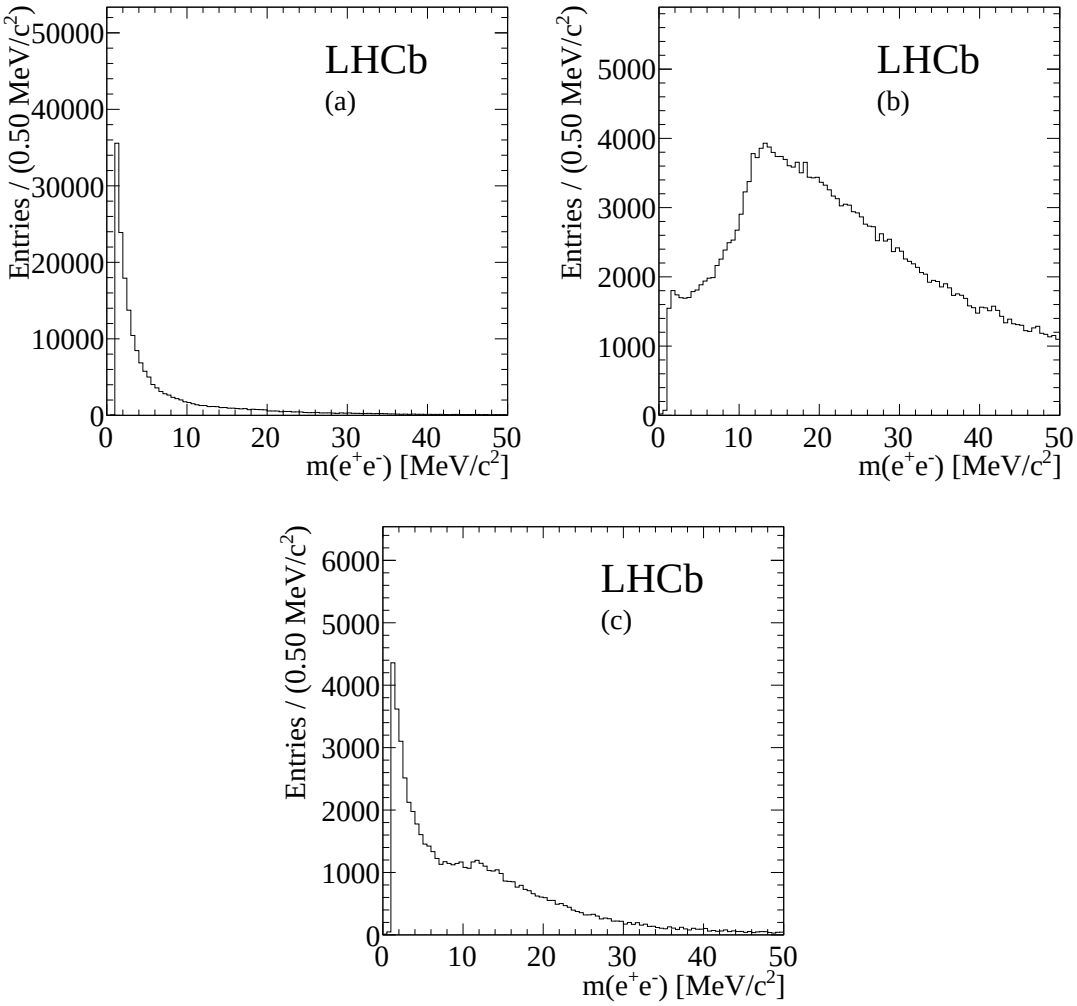

Figure 5: Diphoton invariant mass for background data events for the single long conversion (a), single downstream conversion (b), and double conversion (c) topologies.

[6] S. W. Bosch and G. Buchalla, *The Double radiative decays $B \to \gamma\gamma$ in the heavy quark limit*, JHEP **08** (2002) 054, arXiv:hep-ph/0208202.

[7] G. Barrand *et al.*, *GAUDI - A software architecture and framework for building HEP data processing applications*, Comput. Phys. Commun. **140** (2001) 45.

[8] S. Tolk, J. Albrecht, F. Dettori, and A. Pellegrino, *Data driven trigger efficiency determination at LHCb*, LHCb-PUB-2014-039. CERN-LHCb-PUB-2014-039.

[9] R. Aaij *et al.*, *The LHCb trigger and its performance in 2011*, JINST **8** (2013) P04022, arXiv:1211.3055.

[10] V. V. Gligorov and M. Williams, *Efficient, reliable and fast high-level triggering using a bonsai boosted decision tree*, JINST **8** (2013) P02013, arXiv:1210.6861.

A $B_s^0 \to \gamma\gamma$ BDT inputs

The inputs used to train the the BDTs described in Section 4 are given in this Appendix, where signal and background distributions are normalised to have the same area. The variables used as input to the classifiers consist of:

- the B_s^0 $p_{\rm T}$;
- $p_{\rm T}(\gamma_1) + p_{\rm T}(\gamma_2)$;
- $|p_{\rm T}(\gamma_1) - p_{\rm T}(\gamma_2)|/(p_{\rm T}(\gamma_1) + p_{\rm T}(\gamma_2))$;
- the probability of being a true calorimeter photon (`IsPhoton`) for the case of a single conversion;
- the minimum probability of being a true calorimeter photon for the di-calorimeter photon classifier;
- the minimum $\mathrm{DLL}_{e\pi}$ of the electrons from the photon conversion, where $\mathrm{DLL}_{e\pi}$ is the difference in likelihood between the electron and pion mass hypotheses;
- the minimum probability of not being an electron (`IsNotE`) of the two calorimeter photons;
- the invariant mass of the converted photon for the case of the single long conversion classifier;
- the ratio of the calorimeter photon seed energy to the cluster energy (`CALO shape E1`) for the single long conversion classifier only.

The signal and background distributions of the di-calorimeter photon, single conversion to long electron pairs, single conversion to downstream electron pairs, and double conversion classifiers are shown in Figures 6, 7, 8, 9, respectively.

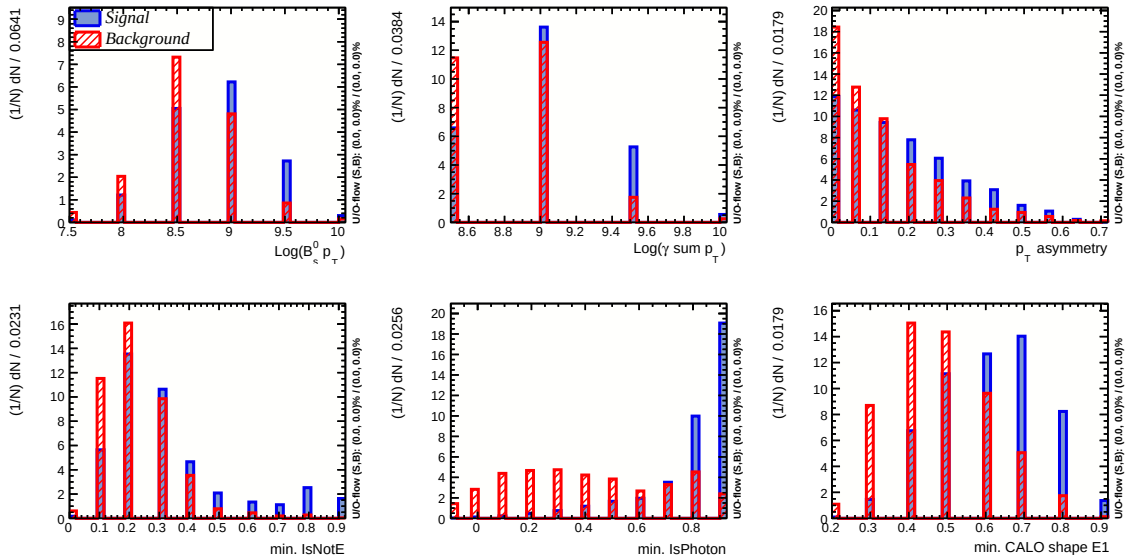

Figure 6: Discretised signal and background distributions used to train the BDT to select $B_s^0 \to \gamma\gamma$ decays in the di-calorimeter photon topology.

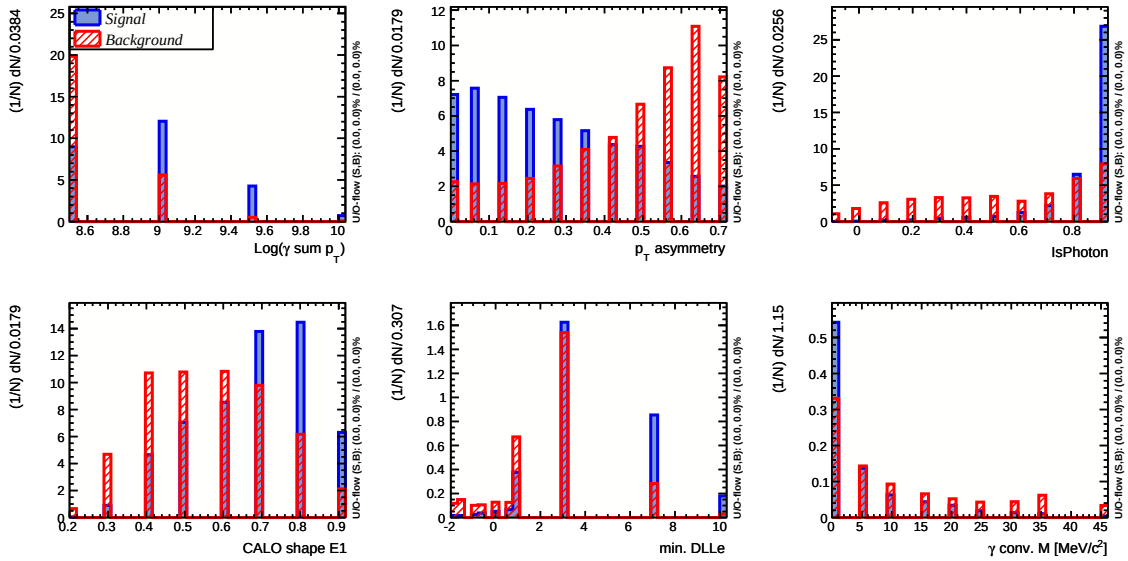

Figure 7: Discretised signal and background distributions used to train the BDT to select $B_s^0 \to \gamma\gamma$ decays in the topology of a single converted photon to a pair of long electrons.

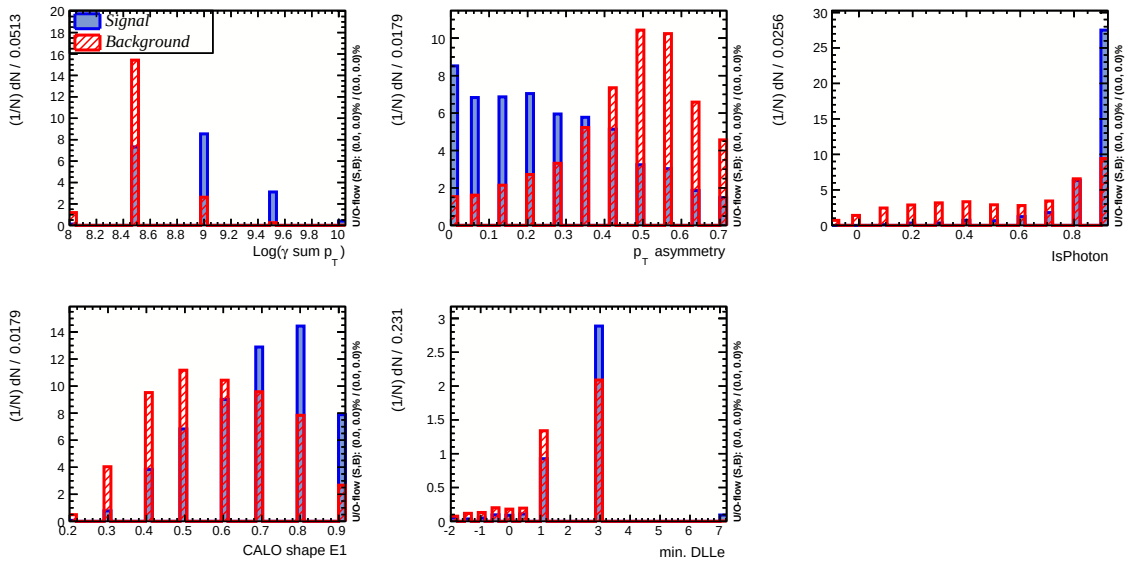

Figure 8: Discretised signal and background distributions used to train the BDT to select $B_s^0 \to \gamma\gamma$ decays in the topology of a single converted photon to a pair of downstream electrons.

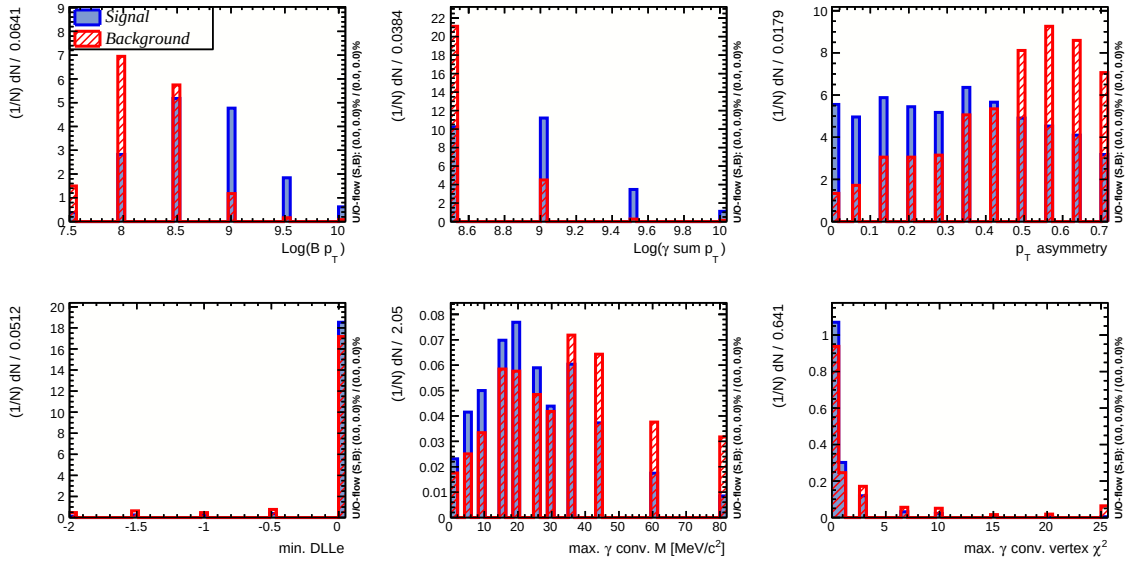

Figure 9: Discretised signal and background distributions used to train the BDT to select $B_s^0 \to \gamma\gamma$ decays in the topology of two converted photons, either long or downstream.